Epigenetic *SMAD3* Repression in Tumor-Associated Fibroblasts Impairs Fibrosis and Response to the Antifibrotic Drug Nintedanib in Lung Squamous Cell Carcinoma

Rafael Ikemori[1], Marta Gabasa[1], Paula Duch[1], Miguel Vizoso[2], Paloma Bragado[3,4], Marselina Arshakyan[1], Iuliana-Cristiana Luis[1], Albert Marín[1], Sebastian Morán[5], Manuel Castro[5], Gemma Fuster[3,4], Sabrina Gea-Sorli[3,6], Toni Jauset[7], Laura Soucek[7,8,9], Luis M. Montuenga[10,11], Manel Esteller[5,8,11,12], Eduard Monsó[13,14], Victor Ivo Peinado[3,13], Pere Gascon[3,4,15], Cristina Fillat[3,4,6], Frank Hilberg[16], Noemí Reguart[3,15], and Jordi Alcaraz[1,13,17]

ABSTRACT

The tumor-promoting fibrotic stroma rich in tumor-associated fibroblasts (TAF) is drawing increased therapeutic attention. Intriguingly, a trial with the antifibrotic drug nintedanib in non–small cell lung cancer reported clinical benefits in adenocarcinoma (ADC) but not squamous cell carcinoma (SCC), even though the stroma is fibrotic in both histotypes. Likewise, we reported that nintedanib inhibited the tumor-promoting fibrotic phenotype of TAFs selectively in ADC. Here we show that tumor fibrosis is actually higher in ADC-TAFs than SCC-TAFs *in vitro* and patient samples. Mechanistically, the reduced fibrosis and nintedanib response of SCC-TAFs was associated with increased promoter methylation of the profibrotic TGFβ transcription factor *SMAD3* compared with ADC-TAFs, which elicited a compensatory increase in TGFβ1/SMAD2 activation. Consistently, forcing global DNA demethylation of SCC-TAFs with 5-AZA rescued TGFβ1/SMAD3 activation, whereas genetic downregulation of *SMAD3* in ADC-TAFs and control fibroblasts increased TGFβ1/SMAD2 activation, and reduced their fibrotic phenotype and antitumor responses to nintedanib *in vitro* and *in vivo*. Our results also support that smoking and/or the anatomic location of SCC in the proximal airways, which are more exposed to cigarette smoke particles, may prime SCC-TAFs to stronger *SMAD3* epigenetic repression, because cigarette smoke condensate selectively increased *SMAD3* promoter methylation. Our results unveil that the histotype-specific regulation of tumor fibrosis in lung cancer is mediated through differential *SMAD3* promoter methylation in TAFs and provide new mechanistic insights on the selective poor response of SCC-TAFs to nintedanib. Moreover, our findings support that patients with ADC may be more responsive to antifibrotic drugs targeting their stromal TGFβ1/SMAD3 activation.

Significance: This study implicates the selective epigenetic repression of *SMAD3* in SCC-TAFs in the clinical failure of nintedanib in SCC and supports that patients with ADC may benefit from antifibrotic drugs targeting stromal TGFβ1/SMAD3.

Introduction

Lung cancer is the most common cause of cancer-related deaths worldwide, with a 5-year survival rate of approximately 18% in developed countries, and smoking and pollution are its major risk factors (1, 2). Histologically, most patients with lung cancer are diagnosed as non–small cell lung cancer (NSCLC, ∼85%), which is further classified into adenocarcinoma (ADC, ∼50%), squamous cell carcinoma (SCC; ∼40%), and other less frequent subtypes (3). Although the latter subtypes are epithelial in origin, it is increasingly acknowledged that tumor-associated fibroblasts (TAF) are essential

[1]Unit of Biophysics and Bioengineering, Department of Biomedicine, School of Medicine and Health Sciences, Universitat de Barcelona, Barcelona, Spain. [2]Division of Molecular Pathology, Oncode Institute, The Netherlands Cancer Institute, Amsterdam, the Netherlands. [3]Institut d'Investigacions Biomèdiques August Pi i Sunyer (IDIBAPS), Barcelona, Spain. [4]Department of Medicine, School of Medicine and Health Sciences, Universitat de Barcelona, Barcelona, Spain. [5]Josep Carreras Leukaemia Research Institute (IJC), Badalona, Barcelona, Spain. [6]Centro de Investigación Biomédica en Red de Enfermedades Raras (CIBERER), Barcelona, Spain. [7]Vall d'Hebron Institute of Oncology (VHIO), Edifici Cellex, Hospital Vall d'Hebrón, Barcelona, Spain. [8]Institució Catalana de Recerca i Estudis Avançats (ICREA), Barcelona, Spain. [9]Department of Biochemistry and Molecular Biology, Universitat Autònoma de Barcelona, Bellaterra, Spain. [10]Program in Solid Tumors, Center for Applied Medical Research Institution (CIMA), University of Navarra, Pamplona, Spain. [11]Centro de Investigación Biomedica en Red de Cáncer (CIBERONC), Instituto de Salud Carlos III, Madrid, Spain. [12]Physiological Sciences Department, School of Medicine and Health Sciences, Universitat de Barcelona, Hospitalet de Llobregat, Barcelona, Spain. [13]Centro de Investigación Biomédica en Red de Enfermedades Respiratorias (CIBERES), Instituto de Salud Carlos III, Madrid, Spain. [14]Respiratory Medicine, Hospital Universitari Parc Taulí, Sabadell, Spain. [15]Medical Oncology Department, Hospital Clínic de Barcelona, Barcelona, Spain. [16]Boehringer Ingelheim Austria RCV GmbH & Co KG, Vienna, Austria. [17]Institute for Bioengineering of Catalonia (IBEC), The Barcelona Institute for Science and Technology (BIST), Barcelona, Spain.

Note: Supplementary data for this article are available at Cancer Research Online (http://cancerres.aacrjournals.org/).

Corresponding Author: Jordi Alcaraz, Unit of Biophysics and Bioengineering, Department of Biomedicine, School of Medicine and Health Sciences, Universitat de Barcelona, Casanova 143, Barcelona 08036, Spain. Phone: 349-3403-1148; Fax: 349-3403-5278; E-mail: jalcaraz@ub.edu

Cancer Res 2020;80:276–90

doi: 10.1158/0008-5472.CAN-19-0637

stromal coconspirators of tumor progression, because they have been implicated in tumor growth, angiogenesis, invasion, immunosuppression, and even therapy resistance (4, 5). Accordingly, dissecting the pathologic functions of TAFs in each cancer subtype has become an active field of research.

Lung TAFs exhibit an activated/profibrotic phenotype in patient samples, as indicated by their overwhelming positivity in histologic stainings for alpha-smooth muscle actin (αSMA), fibrillar collagens, and other standard fibroblast activation markers, which underlines that the stroma of NSCLC is markedly fibrotic (6, 7). Moreover, these fibrosis markers have been associated with low survival (7). Likewise, the potent fibroblast activator cytokine TGFβ1 (8), which is often upregulated in NSCLC, has also been associated with poor prognosis (9). Paradoxically, we recently reported that *SMAD3*, which is an important profibrotic transcription factor of the TGFβ pathway (10), was epigenetically downregulated through promoter hypermethylation in lung TAFs compared with patient-matched control fibroblasts (11). In addition, we reported that the clinically approved antifibrotic drug nintedanib elicited a stronger inhibition of both the profibrotic phenotype and its associated tumor-promoting effects in ADC-TAFs compared with SCC-TAFs upon TGFβ1 stimulation *in vitro* (12), which was consistent with the selective therapeutic response to nintedanib observed in the LUME-1 clinical trial in patients with ADC (but not SCC; ref. 13). Altogether, these previous results support the hypothesis that TGFβ1/SMAD3 signaling goes awry in lung TAFs, and that such alteration may depend on the histologic subtype, which could be associated with the distinct nintedanib effects in ADC and SCC. To test this hypothesis, we examined the expression and activation of SMAD3 and its closely related homolog SMAD2 in TAFs and paired control fibroblasts, and the potential mechanisms underlying the *SMAD3* promoter hypermethylation in TAFs. Furthermore, we determined the potential contribution of SMAD3 to the differential therapeutic responses to nintedanib observed in ADC and SCC.

Materials and Methods

Tissue samples and primary fibroblasts

Primary pulmonary fibroblasts were previously derived from a cohort of 22 NSCLC surgical patients (11 ADC, 11 SCC; ref. 14; UB-Clinic cohort). Fibroblasts were obtained from tumor (TAF) and paired-uninvolved pulmonary samples [used as control fibroblasts (CF)] with the approval of the Ethics Committee of the Hospital Clinic de Barcelona and the Universitat de Barcelona. Fibroblasts were characterized by their expression of vimentin, and lack of expression of cytokeratins, as we demonstrated elsewhere (11). Selected patients were male, chemo- and radiotherapy-naïve, Caucasian, ≥55-year-old, and current smokers (further details in Supplementary Table S1). TMAs previously gathered by the CIBERES/Spanish Bronchogenic Carcinoma Cooperative Group (CIBERES cohort; $n = 208$; 112 ADC, 96 SCC; ref. 7) and by the CIMA-Clínica Universidad de Navarra (CIMA-CUN cohort; $n = 131$; 77 ADC, 54 SCC) with the approval of the Ethics Committee of the Fundació Parc Taulí and Clínica Universidad de Navarra (Navarra, Spain), respectively, were used for IHC. TMA patients were Caucasian and did not receive radiotherapy prior to surgery, because radiotherapy may induce unwanted pulmonary fibrosis (15). Written informed consent was obtained from all patients in all cohorts, and all protocols used were in accordance with the Declaration of Helsinki. A summary of patient clinicopathologic variables is shown in Supplementary Table S2.

Histologic analysis

Tissue microarrays (TMA) samples were prepared as described (7), and analyzed in terms of fibrosis markers by examining fibrillar collagens and αSMA by picrosirius red (PSR) and IHC, respectively. Primary tumor xenografts obtained from *in vivo* studies were formalin fixed (Merck Millipore), paraffin embedded (Paraplast, Sigma), sliced in 2-μm sections, and analyzed in terms of fibrosis (αSMA and fibrillar collagens) and proliferation (Ki-67; #M7240, DAKO) markers. Nuclei were counterstained with hematoxylin. αSMA, PSR, and Ki-67 stainings were imaged with an upright microscope (BX43) coupled to a digital camera (DP72, Olympus) using a 10× objective for TMAs and a 20× objective for tumor xenografts. Image processing was carried out here and thereafter with ImageJ (16). Images were color deconvoluted, binarized, and used to calculate the positive area fraction (%), which was averaged for each patient. The number of Ki-67–positive nuclei/image was counted and averaged for each condition.

Two-photon microscopy

Collagen fibers were imaged by second harmonic generation (SHG) adapting a previous protocol (17). SHG images were analyzed with CT-FIRE (18) to automatically detect individual collagen fibers (further details in Supplementary Materials).

Cell culture and fibroblast immortalization

Primary fibroblasts were used up to passage 6. Fibroblast experiments were performed on fibroblast culture medium containing serum-free high-glucose DMEM supplemented with 1% ITS and antibiotics as reported previously (12). Fibroblasts were seeded overnight and activated with 2.5 ng/mL TGFβ1 (R&D Systems) during 30 minutes, 60 minutes, or 2–3 days depending on the experiment. Unless otherwise indicated, all fibroblasts were treated with TGFβ1 to regain the activated phenotype observed in histologic samples (7), which is partially lost in culture (11). In some experiments, fibroblasts were stimulated with TGFβ1 in the presence of nintedanib (Boehringer Ingelheim, provided by Frank Hilberg), SB431542 (Millipore) or galunisertib (Lilly, provided by Kyla Driscoll). For DNA demethylation experiments, SCC-TAFs and CFs were seeded at 1.2×10^4 cells/cm^2 density in fibroblast culture medium supplemented with 10% FBS (Gibco) for 4 hours, and treated daily with 0.5 or 1.5 μmol/L 5-azacytidine (5-AZA, Sigma) or vehicle (DMSO; Sigma) for 4 days. Afterwards, cells were kept in fibroblast culture medium for 8 hours, and stimulated with 2.5 ng/mL TGFβ1 for 1 hour. For immunofluorescence studies, fibroblasts were seeded overnight in fibroblast culture medium in collagenated culture slides (BD Falcon), stimulated with 2.5 ng/mL TGFβ1 in the presence of 2 μmol/L nintedanib, 10 μmol/L SB431542, or vehicle for 1 hour. Fibroblasts from randomly selected patients were immortalized with hTERT (further details in Supplementary Materials and Methods; ref. 5). ADC cell line H1437 (ATCC) was maintained in RPMI1640-based medium as described previously (12), and used up to passage 12 after thawing. Primary cultures and cell lines were confirmed to be negative for *Mycoplasma* using the MycoAlert Mycoplasma Detection Kit (Lonza).

Knockdown of SMAD2 and SMAD3 in primary fibroblasts

SMAD2 and SMAD3 were stably knocked down with lentiviral vectors from the Sigma MISSION collection, shRNA for SMAD2 and SMAD3. A nonmammalian targeting shRNA vector was used as control (SHC002). Briefly, HEK293T cells (ATCC CRL-3216) were transfected with suitable plasmids, and their supernatant containing lentivirus was filtered and used to transduce hTERT-immortalized

fibroblasts. Transduced cells were selected with puromycin (Sigma; more details in Supplementary Materials).

SMAD3 and *SMAD2* pyrosequencing

SMAD3 and *SMAD2* pyrosequencing was conducted using bisulfite-treated DNA as a template for PCR as described previously (11). Primer sequences (Supplementary Materials and Methods) were designed to hybridize CpG-free sites to ensure methylation-independent amplification. Pyrosequencing analyses were conducted on 3 CpG sites for *SMAD3* (11), and on 4 CpG sites for *SMAD2* (additional information in Supplementary Materials).

Cigarette smoke condensate

Cigarette smoke condensate (CSC) was produced as described (19). Immortalized CFs were cultured in complete medium with increasing CSC concentrations (5%, 6.7%, and 10%, which correspond to 1:20, 1:15, and 1:10 dilutions, respectively) up to 6 weeks, replacing the CSC-containing medium three times/week (further details in Supplementary Materials).

Conditioned medium from TAFs

TAFs were activated with serum-free fibroblast culture medium supplemented with 2.5 ng/mL TGFβ1 in the presence or absence of 2 μmol/L nintedanib for 3 days, kept in serum-free medium for 2 days in the absence of exogenous TGFβ1, and the corresponding conditioned medium (CM) was collected (12). Carcinoma cell growth upon CM stimulation was assessed as cell number/image field (12).

TGFβ activity reporter assay

The activity of bioactive TGFβ was monitored using the TGFβ-inducible $p(CAGA)_{12}$ luciferase reporter as described previously (additional information in Supplementary Materials; ref. 20).

qRT-PCR

The fibrotic phenotype was assessed by qRT-PCR in technical duplicates with the StepOnePlus Real-Time PCR System (Applied Biosystems) using Taqman probes for *COL1A1, COL3A1, TGFB1*, and *POL2R* (used as endogenous control) and Taqman Master Mix (Thermo Fisher Scientific) as reported previously (12). To evaluate the expression of R-SMAD2/3, qRT-PCR analysis was performed using specific primers for *SMAD2, SMAD3*, and *ACTB* (used as endogenous control) and SYBR Green Master Mix (Thermo Fisher Scientific). Relative expression with respect to an endogenous control was computed as $2^{-\Delta C_t}$ (more details in Supplementary Materials; ref. 21).

Western blot analysis

Protein extraction was performed with a lysis buffer containing Tris 50 mmol/L pH 7.4, NaCl 150 mmol/L, SDS 0.1%, Triton X-100 1% (Sigma), Nonidet P-40 1% (Igepal), proteinase (Cocktail Set I, Merck; Pefabloc, Roche), and phosphatase (Phostop, Roche) inhibitors. Equal protein amounts were separated with precast gels, transferred to a polyvinylidene difluoride membrane as described previously (12), blocked, and incubated overnight with primary antibodies against pSMAD2 (#3101, Cell Signaling Technology), pSMAD3 (#07-1389, Merck Millipore), P4HA2 (#13758-1-AP, ProteinTech), αSMA (#A5228, Sigma-Aldrich), β-actin (#A1978, Sigma-Aldrich), and α-tubulin (#2144, Cell Signaling Technology). Protein bands were labeled, visualized by chemiluminescence (Imagequant LAS4000, GE Healthcare), and band intensities were analyzed with ImageJ and normalized to the corresponding loading control.

Immunofluorescence

Immunofluorescence staining of nuclear SMAD4 was performed adapting protocols reported elsewhere (further details in Supplementary Materials; ref. 22).

In vivo tumorigenicity

The tumorigenicity of ADC cancer cells mixed with fibroblasts was examined in 4- to 6-week-old male NOD/SCID mice (Charles River), using protocols approved by the Animal Care and Ethics Committee of the University of Barcelona (Barcelona, Spain). Fibroblasts (control shRNA CF^{hTERT} or shSMAD3 CF^{hTERT}; #5) were preactivated with 2.5 ng/mL TGFβ1 for 3 days before coinjection. H1437 cells (0.5×10^6) were mixed with either control shRNA or shSMAD3 CF^{hTERT} (#5; 1×10^6) within 100 μL solution of Matrigel (BD Biosciences) and type I collagen (IAC-50, Koken; 1:1) and coinjected subcutaneously in the dorsal flank of the NOD/SCID mice. Tumor growth was computed as $0.5 \times \text{width}^2 \times \text{length}$ using calipers (23). Once tumor volume was ≥ 50 mm^3, animals were treated with nintedanib diluted in sterile PBS administered daily by oral gavage at 50 mg/kg body weight, whereas PBS was used as a control ($n = 6$/condition). The percentage of tumor-free mice was assessed using a tumor threshold (size < 200 mm^3; ref. 23). After 14 days, animals were euthanized with 4 mg/kg ketamine (Richter Pharma) and 0.4 mg/mL xylazine (Bayer) followed by cervical dislocation, and the tumor xenografts were collected.

The Cancer Genome Atlas data analysis

Level 3 RNA-seq data and clinical information about patients with NSCLC were downloaded from The Cancer Genome Atlas (TCGA) project (https://cancergenome.nih.gov/) and analyzed using the RNA-Seq by Expectation Maximization (RSEM) with the RTCGA package (https://rtcga.github.io/RTCGA). Selected patients were Caucasian, never or current/former smokers, and without previous radiotherapy to match the patient characteristics of the other cohorts.

Statistical analysis

Two-group comparisons were performed with two-tailed Student *t* test unless otherwise indicated. Tumor volume and the percentages of tumor-free mice with or without nintedanib were compared with two-way ANOVA and log-rank test, respectively (GraphPad Prism v5.0.). TMA data (PSR% and αSMA%) were analyzed with R-software (v3.4.0) by assessing their degree of linear association through the Pearson correlation coefficient. A linear model between PSR% and αSMA% was estimated with the intercept set at 0, in which the interaction of the slope with the histologic subtype was examined using the likelihood ratio test. Statistical significance was assumed at $P < 0.05$. All data shown are mean ± SE.

Results

The aberrant expression and activation of SMAD2 and SMAD3 in lung TAFs depend strongly on their histologic subtype

TGFβ1 signaling begins with its binding to type II TGFβ receptor, which phosphorylates type I TGFβ receptor ALK5, which subsequently phosphorylates SMAD2 and SMAD3 (referred to as receptor-activated SMAD2/3 or R-SMAD2/3), upon which they form heterotrimeric complexes with the cofactor SMAD4 that translocate to the nucleus to regulate gene expression (24, 25). To check whether R-SMAD2/3 were functional, we stimulated TAFs from randomly selected patients ($n = 4$) with TGFβ1 in the presence of the ALK5 inhibitor SB431542 (26). TGFβ1 markedly increased

the phosphorylation of SMAD3 (pSMAD3) and SMAD2 (pSMAD2; **Fig. 1A**), and the nuclear SMAD4 translocation (**Fig. 1B** and **C**; Supplementary Fig. S1A), concomitantly with a panel of fibrotic markers, including αSMA, prolyl-4-hydroxylase α subunit 2 (P4HA2; **Fig. 1D**; Supplementary Fig. S1B), an essential enzyme for collagen biosynthesis (27), and fibrillar collagen *COL1A1* (**Fig. 1E**). Conversely, SB431542 prevented the TGFβ1-induced increases in the activation of R-SMAD2/3 (**Fig. 1A**), nuclear SMAD4 (**Fig. 1B** and **C**), and expression of fibrosis markers (**Fig. 1D** and **E**; Supplementary Fig. S1A and S1B), thereby confirming that R-SMAD2/3 are activated by TGFβ1, and are functional in terms of upregulating fibrotic markers.

To test our hypothesis that TGFβ1/SMAD3 signaling could be dysfunctional in an histotype-dependent fashion, we first examined the mRNA and total protein expression and phosphorylation of R-SMAD2/3 in TAFs in response to TGFβ1 with respect to patient-matched CFs from randomly selected patients ($n = 10$ for mRNA, $n = 13$ for protein analysis). Intriguingly, we found differences in R-SMAD2/3 between ADC-TAFs and SCC-TAFs consistently at both the mRNA (**Fig. 1F–H**) and total protein levels (Supplementary Fig. S1C–F), and even more differences at the phosphorylation level. In SCC-TAFs, *SMAD3* mRNA (**Fig. 1F**) and pSMAD3 (**Fig. 1I** and **J**; Supplementary Fig. S1G) were significantly downregulated with respect to CFs, in agreement with our previously reported epigenetic downregulation of *SMAD3* in TAFs (11). Conversely, *SMAD2* mRNA (**Fig. 1G**) remained unaltered in all groups. In contrast, pSMAD2 was significantly increased in SCC-TAFs with respect to CFs (**Fig. 1I** and **K**). The latter results were not expected given the similar *SMAD2*

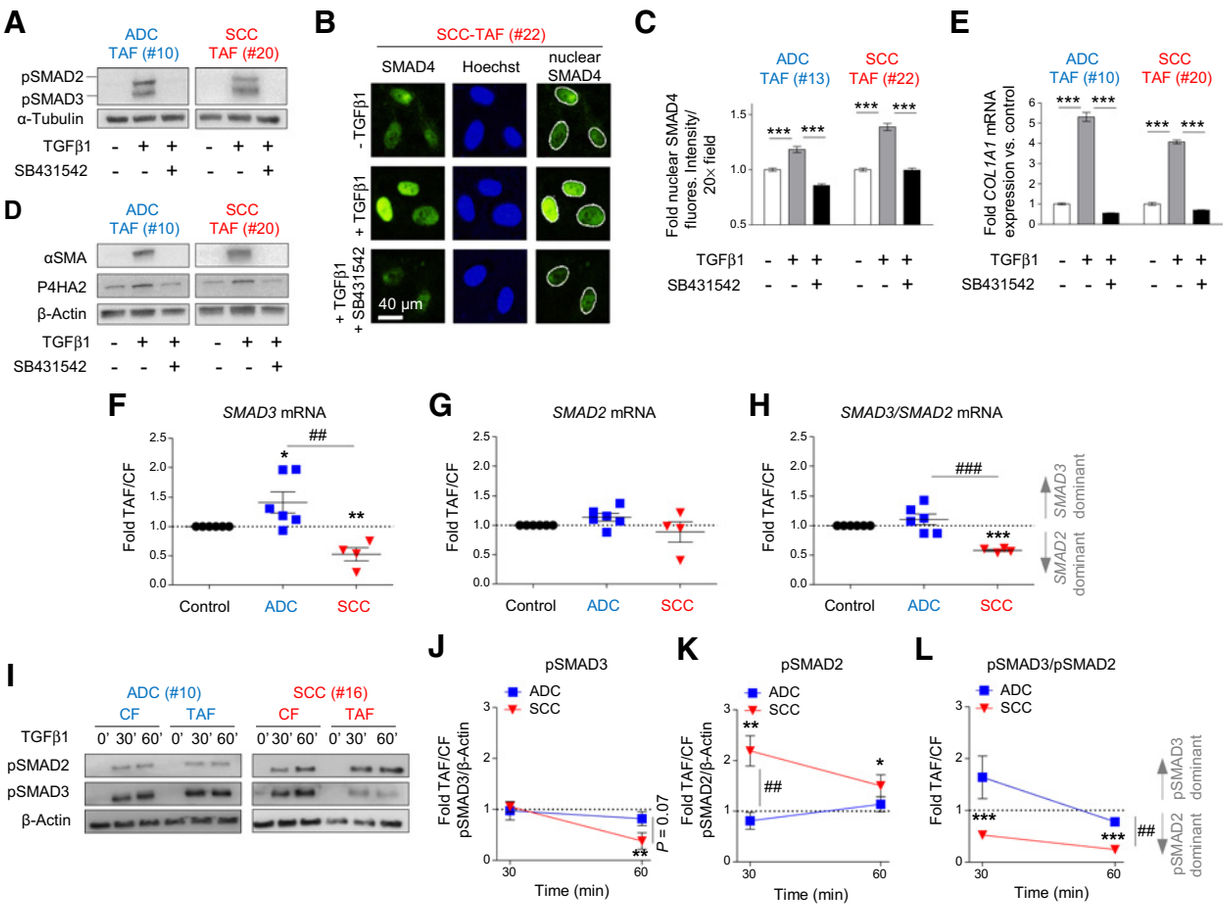

Figure 1.

Subtype-specific imbalance of R-SMAD2/3 in lung TAFs. **A,** Representative Western blot of pSMAD2, pSMAD3, and α-tubulin in ADC-TAFs (patient #10) and SCC-TAFs (patient #20) stimulated with 2.5 ng/mL TGFβ1 with or without 10 μmol/L SB431542 for 60 minutes (additional Western blot is shown in Supplementary Fig. S1B). **B** and **C,** Representative immunofluorescence images of nuclear SMAD4 of TAFs (**B**) cultured as in **A** and corresponding quantification (**C**). **D** and **E,** Representative Western blot for αSMA, P4HA2, and β-actin (**D**) and fold *COL1A1* mRNA levels (**E**) of TAFs cultured as in **A** for 3 days. **F, G,** and **H,** Fold (TAF/CF) mRNA expression of *SMAD3* (**F**), *SMAD2* (**G**), and *SMAD3/SMAD2* (**H**) ratio of ADC ($n = 6$; TAFs and CFs) and SCC ($n = 4$; TAFs and CFs) fibroblasts cultured as in **D**. **I,** Representative Western blot of phosphorylated R-SMAD2/3 and β-actin in TAFs and paired CFs from patients with ADC and SCC upon 2.5 ng/mL TGFβ1 stimulation for 30–60 minutes (additional Western blot is shown in Supplementary Fig. S1G–S1H; quantification in Supplementary Tables S3 and S4). **J, K,** and **L,** Densitometry analysis of pSMAD3/β-actin (**J**), pSMAD2/β-actin (**K**), and pSMAD3/pSMAD2 ratio (**L**) in primary fibroblasts cultured as in **I**, derived from patients with ADC ($n = 8$; TAFs and CFs) and SCC ($n = 5$; TAFs and CFs). #, $P < 0.05$; ##, $P < 0.01$; ###, $P < 0.005$ comparing ADC and SCC by Student *t* test here and thereafter; *, $P < 0.05$; **, $P < 0.01$; ***, $P < 0.005$ comparing either TAFs and CFs, or TAFs treated or untreated with SB431542, by Student *t* test.

mRNA (**Fig. 1G**) and total SMAD2 protein levels (Supplementary Fig. S1C–S1F) observed in SCC-TAFs and CFs, yet they are consistent with a regulatory process of the relative activation of SMAD2 and SMAD3 based on their competition for common factors (28, 29). As a result of the imbalance in R-SMAD2/3, both the *SMAD3*/*SMAD2* mRNA ratio (**Fig. 1H**) and the pSMAD3/pSMAD2 activation ratio (**Fig. 1L**) were significantly low (<1) in SCC-TAFs with respect to paired CFs.

Surprisingly, ADC-TAFs exhibited opposite expression and activation patterns of R-SMAD2/3 compared with SCC-TAFs. Thus, *SMAD3* mRNA (**Fig. 1F**) was higher in ADC-TAFs compared with SCC-TAFs and CFs. Likewise, we observed a significantly opposite activation of SMAD3 and SMAD2 in ADC-TAFs compared with SCC-TAFs (**Fig. 1I–K**; Supplementary Fig. S1H). These differences elicited significantly higher *SMAD3*/*SMAD2* mRNA ratio (**Fig. 1H**) and pSMAD3/pSMAD2 ratio (**Fig. 1L**) in ADC-TAFs with respect to SCC-TAFs. The total (Supplementary Fig. S1F) and phosphorylated (**Fig. 1L**) SMAD3/SMAD2 protein ratios of ADC-TAFs were also higher than paired CFs (i.e., >1) at early time points, although these differences did not attain statistical significance. These results show that TGFβ1 responses are dominated by pSMAD2 over pSMAD3 in SCC-TAFs, and inversely (i.e., by pSMAD3 over pSMAD2) in ADC-TAFs, thereby indicating that the balance between R-SMAD2/3 expression and/or signaling in TAFs is strongly associated with their histologic subtype.

DNA hypermethylation of the SMAD3 promoter in TAFs is subtype-dependent and is environmentally regulated by CSC in CFs

To shed light on the apparent discrepancy between the subtype-dependent differences in *SMAD3* mRNA levels in ADC-TAFs and SCC-TAFs, and our previously reported epigenetic repression of *SMAD3* in TAFs regardless their histologic subtype, we reanalyzed our *SMAD3* promoter methylation data in TAFs and paired CFs from 12 patients (6 ADC, 6 SCC) assessed by pyrosequencing in three CpG sites (Supplementary Fig. S2A and S2B; ref. 11). In agreement with our initial observations (11), *SMAD3* promoter methylation was significantly higher in both ADC-TAFs and SCC-TAFs compared with paired CFs. Yet, this difference was markedly larger in SCC-TAFs (**Fig. 2A**), which is consistent with their lowest *SMAD3* mRNA expression (**Fig. 1F**). In contrast, the overexpression of *SMAD3* mRNA in ADC-TAFs with respect to CFs was unexpected (**Fig. 1F**), for its promoter was slightly hypermethylated compared with CFs, thereby suggesting that transcriptional regulatory processes other than DNA methylation are involved.

To further support a causal relationship between increased *SMAD3* promoter methylation and *SMAD3* transcriptional repression in SCC-TAFs, we treated SCC-TAFs and paired CFs from randomly selected patients ($n = 2$) with the global DNA demethylating agent 5-AZA, which inhibits the maintenance enzyme DNA methyltransferase DNMT1 (30), and found a significant dose-dependent decrease in *SMAD3* promoter methylation of both SCC-TAFs and paired CFs with respect to control, although it was more pronounced in the former (**Fig. 2B** and **C**; Supplementary Fig. S2C). Yet, this demethylation was sufficient to dose-dependently increase the fold *SMAD3* mRNA (**Fig. 2D** and **E**) and the TGFβ1-induced pSMAD3 significantly in TAFs, but not in CFs (**Fig. 2F–H**; Supplementary Fig. S2D–S2F). Similar results were found in CFs from other patients (Supplementary Fig. S2F), confirming that 5-AZA could rescue the expression and TGFβ1-induced activation of SMAD3 in SCC-TAFs but not in CFs, in agreement with the highest *SMAD3* promoter methylation of SCC-TAFs (**Fig. 2A**).

In addition, we wondered about the potential driving processes of such marked and selective *SMAD3* promoter hypermethylation of SCC-TAFs. Prompted by previous *in vitro* associations of smoking with *SMAD3* mRNA downregulation through histone deacetylation in lung cancer cells (31), by the fact that TAFs and CFs were derived from smokers, and by the common anatomic location of SCC in the proximal airways (3), which are more exposed to cigarette smoke particles (32), we first examined the impact of long-term exposure to CSC. Treating immortalized CFs for 6 weeks with 10% CSC did not alter their morphology (**Fig. 2I**), yet it time dependently increased their *SMAD3* promoter methylation (**Fig. 2J**). Likewise, CSC dose-dependently increased the *SMAD3* promoter methylation of CFs compared with vehicle after 6 weeks (**Fig. 2K**) and even 3 weeks (Supplementary Fig. S2G). In contrast, CSC had no effect on the *SMAD2* promoter methylation (**Fig. 2L** and **M**). These results reveal that CSC is sufficient to hypermethylate the same CpG sites within the *SMAD3* promoter in pulmonary fibroblasts that were hypermethylated in TAFs. To further support a link between smoking and *SMAD3* promoter methylation, we reanalyzed our methylation data in CFs by stratifying patients based on their tobacco consumption, and found increased *SMAD3* promoter methylation in the group with the highest number of cigarette pack-year that reached marginal significance, probably due to the limited patient number (**Fig. 2N**).

The extent of TAF activation *in vitro* and tumor fibrosis *ex vivo* is subtype-specific

Even though SMAD3 and SMAD2 exhibit structural similarities and some overlapping functions, SMAD3 has been pointed selectively as an essential transcription factor of the TGFβ-induced fibrotic responses in fibroblasts (10). Accordingly, given the lower expression and activation of SMAD3 with respect to SMAD2 in SCC-TAFs compared with ADC-TAFs, we expected SCC-TAFs to express lower levels of fibrotic markers compared with ADC-TAFs. In agreement with this hypothesis, we observed a significantly lower expression of a panel of fibrosis markers (αSMA, P4HA2, and *COL1A1*; **Fig. 3A–D**; Supplementary Fig. S3A–S3C) in response to TGFβ1 in SCC-TAFs with respect to ADC-TAFs in randomly selected patients (6 ADC, 5 SCC; all normalized to paired CFs). Moreover, ADC-TAFs significantly overexpressed all fibrosis markers compared with patient-matched CFs, in line with the larger pSMAD3/pSMAD2 ratio of ADC-TAFs with respect to CFs (**Fig. 1L**). The mechanisms underlying such hypertrophic phenotype in ADC-TAFs remain undetermined. However, previous evidence support that TGFβ autoinduction could be involved, because TGFβ1 enhanced selectively the expression of total SMAD3 and SMAD4 in pulmonary fibroblasts (33), and TGFβ autoinduction in turn was critically regulated by SMAD3 in fibroblasts (34). To explore this possibility, we assessed the expression and activity of TGFβ1 by qRT-PCR and the $p(CAGA)_{12}$-luciferase reporter (20), respectively. TGFβ1 mRNA was moderately upregulated in ADC-TAFs compared with SCC-TAFs or CFs upon 72-hour treatment with 2.5 ng/mL TGFβ1 (**Fig. 3E**), and this difference became much larger and statistically significant when analyzing TGFβ activity elicited by the conditioned medium of TAFs (**Fig. 3F**). These results unveil that the abnormally high *SMAD3* expression and activity of ADC-TAFs is associated with an enhanced autoinduction of the profibrotic cytokine TGFβ1.

To validate in patient samples our *in vitro* observation of larger fibrosis in ADC-TAFs compared with SCC-TAFs, we examined two independent TMAs (CIBERES, $n = 208$ and CIMA-CUN, $n = 131$) in

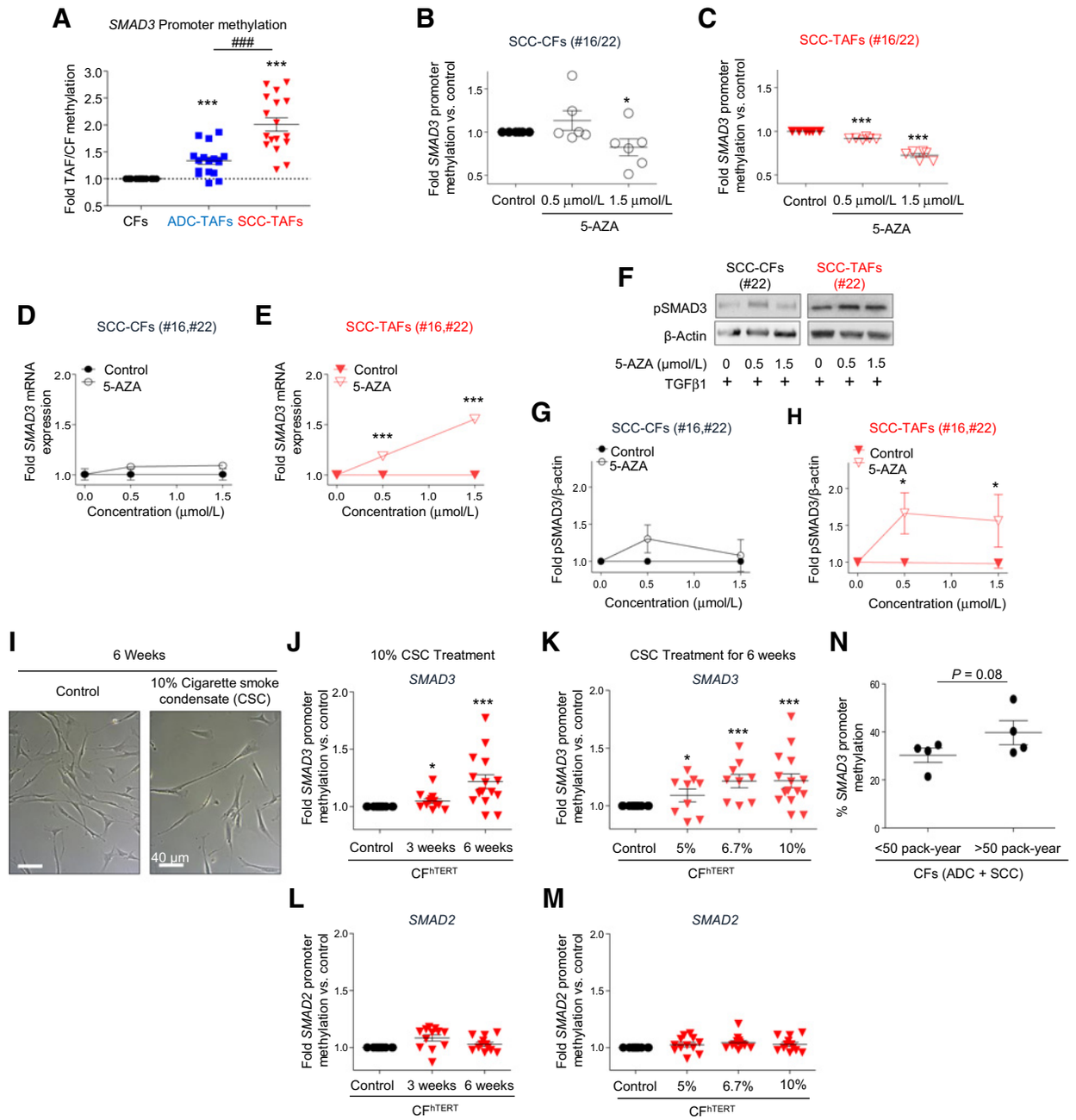

Figure 2.

Epigenetic regulation of *SMAD3* in SCC-TAFs and its relationship with smoking. **A,** Fold (TAF/CF) methylation of the *SMAD3* promoter of primary fibroblasts derived from patients with ADC ($n = 6$; TAFs and CFs) and SCC ($n = 6$; TAFs and CFs) assessed by pyrosequencing in three CpG sites. Because no statistical differences were found among the CpG sites (Supplementary Fig. S2A and S2B), they were used as technical replicates here and thereafter. **B** and **C,** Fold *SMAD3* promoter methylation of paired CFs (**B**) and SCC-TAFs (**C**) from randomly selected patients ($n = 2$) treated with 5-AZA or DMSO vehicle for 4 days and with 2.5 ng/mL TGFβ1 for 1 hour. **D** and **E,** Fold increase in *SMAD3* mRNA in paired CFs (**D**) and SCC-TAFs (**E**) cultured as in **B**. **F,** Representative Western blot of pSMAD3 of SCC-TAFs and paired CFs cultured as in **B**. **G** and **H,** Densitometry analysis of pSMAD3 in paired CFs (**G**) and SCC-TAFs (**H**) cultures as in **F**. Data from other patients shown in Supplementary Fig. S2F. **I,** Representative phase contrast images of CF^{hTERT} (#5) cultured with fibroblast medium supplemented with 10% CSCs and 10% FBS for 6 weeks. **J–M,** Time- and dose-dependent effects of CSC on the fold *SMAD3* (**J** and **K**) and *SMAD2* (**L** and **M**) promoter methylation in CF^{hTERT} (#5) cultured as in **I**. **N,** Pyrosequencing data of the *SMAD3* promoter in CFs (ADC and SCC; $n = 8$) stratified according to the median tobacco consumption. Mean values correspond to $n \geq 3$ independent experiments (**J–M**). Statistical analyses as in **Fig. 1**. *, $P < 0.05$; ***, $P < 0.005$, comparing fibroblasts treated with either 5-AZA or CSCs with their corresponding control.

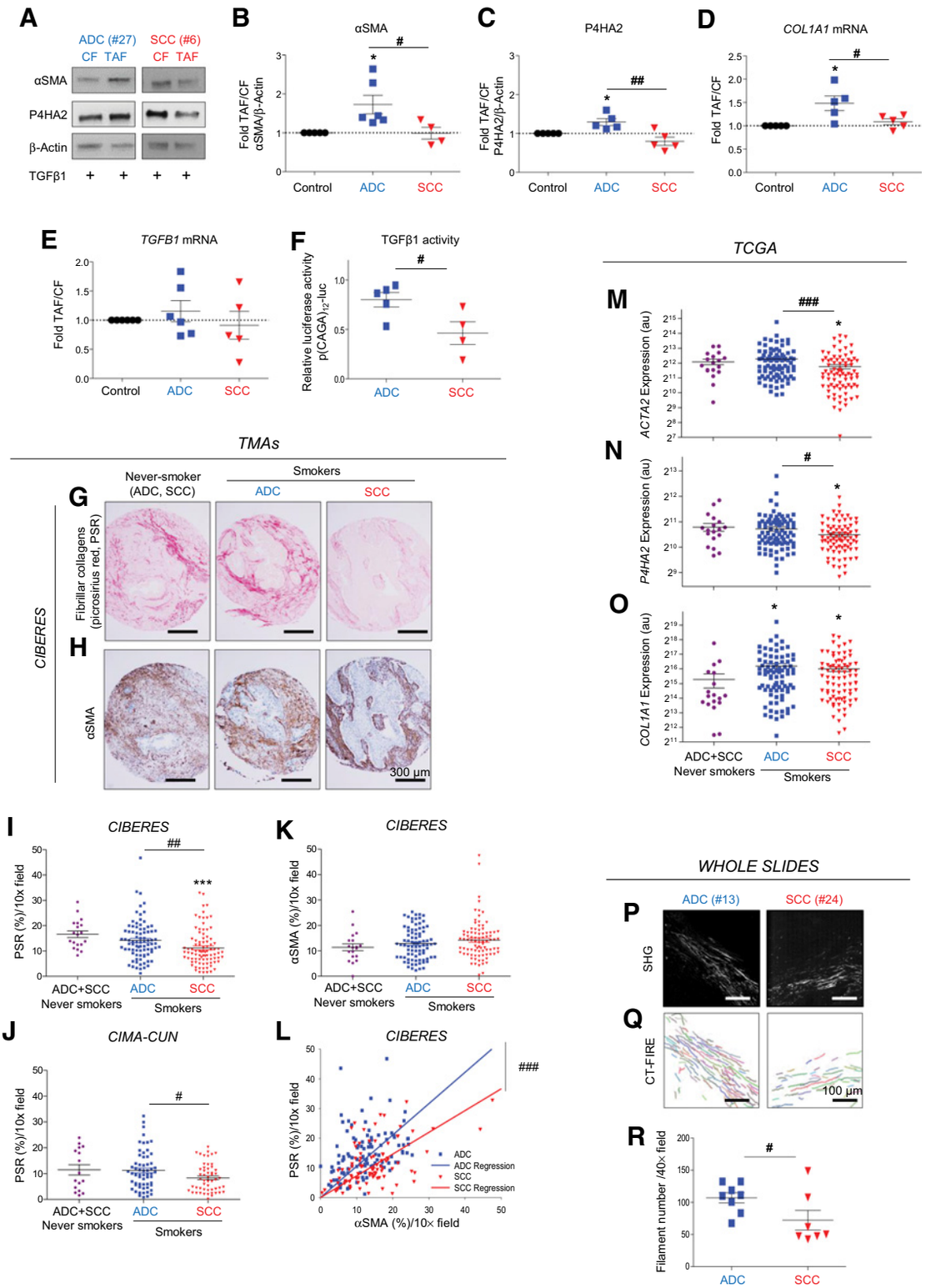

terms of the staining of two fibrosis markers: fibrillar collagens (CIBERES and CIMA-CUN) and αSMA (CIBERES) by PSR and IHC, respectively (**Fig. 3G** and **H**), using quantitative image analysis. To further examine the association between fibrosis and smoking, patients were stratified in three groups: never smokers with ADC or SCC, ADC-smokers, and SCC-smokers (current and former). The average percentage (%) of positively stained PSR area (PSR%) was significantly lower in SCC-smokers compared with ADC-smokers in both cohorts (**Fig. 3G, I, J**), as well as to never smokers in the CIBERES cohort (**Fig. 3I**). Likewise, although the percentage of αSMA–stained area (αSMA%) was comparable among never smokers and smokers in both histotypes (**Fig. 3H** and **K**), plotting PSR% against αSMA% revealed a significantly higher linear slope in ADC than SCC ($P < 0.005$; **Fig. 3L**), indicating that a similar coverage of activated/profibrotic TAFs in both histotypes is associated with more deposition of fibrillar collagens in ADC than SCC. A comparable trend of lower levels of fibrosis markers in SCC-smokers compared with both ADC-smokers (*ACTA2*, which encodes for αSMA, *P4HA2, COL1A1*) and never-smokers (*ACTA2, P4HA2*) was found when analyzing RNA-seq data from the TCGA ($n = 182$; **Fig. 3M–O**), using patient selection criteria that matched those used in the TMAs. TCGA data also revealed a higher expression of *COL1A1* in ADC-smokers compared with never smokers (**Fig. 3M** and **O**), further supporting the hypertrophic nature of ADC-TAFs. Finally, we assessed the number of collagen fibers in whole slides from random patients within the UB-Clinic cohort (8 ADC, 7 SCC) by analyzing SHG images (**Fig. 3P–R**) with CT-FIRE (17), and found a significantly higher number of fibers in ADC compared with SCC (**Fig. 3R**). Altogether, our *in vitro* and *ex vivo* results unveil for the first time intrinsic differences in tumor fibrosis in ADC and SCC, and support a histotype-dependent association between smoking and stromal fibrosis in NSCLC.

Modulation of pSMAD3/pSMAD2 ratio in control fibroblasts phenocopies the subtype-specific activation of TAFs in response to TGFβ1

To further establish a link between the differential expression of fibrosis markers in ADC-TAFs and SCC-TAFs, and their inverted ratios in SMAD3/SMAD2 expression and activation, we used loss-of-function assays of R-SMAD2/3. First, we knocked-down *SMAD3* or *SMAD2* in immortalized CFs from 2 random patients (CF^{hTERT} #5 and #13) by shRNA, whereas a control shRNA against a nonmammalian target was used as a control. A knockdown rather than a knockout approach (34) was used to mimic more faithfully the R-SMAD2/3 differences in TAFs (**Fig. 1F** and **G**). Knocking down SMAD2 in CF^{hTERT} (#5) significantly increased their ratio of both *SMAD3*/*SMAD2* mRNA (**Fig. 4A**) and pSMAD3/pSMAD2 (**Fig. 4B** and **C**) above control shRNA in response to TGFβ1, and such increase was sufficient to upregulate the expression of fibrosis markers (αSMA, P4HA2 and *COL1A1*) compared with control (**Fig. 4D–G**). Conversely, knocking down SMAD3 had the opposite effects (**Fig. 4A–G**). Comparable results were obtained using different shRNA plasmids (shSMAD2B, shSMAD3B; Supplementary Fig. S4A–S4E) and a different patient (CF^{hTERT} #13; Supplementary Fig. S4F–J). Because the differences in the fibrotic responses between shSMAD2 and shSMAD3 CF^{hTERT} to TGFβ1 phenocopied qualitatively those observed between ADC-TAFs and SCC-TAFs, shSMAD2 and shSMAD3 models were referred to as ADC-like and SCC-like, respectively, here and thereafter. Second, we benefited from the differential impact of TGFβ inhibitors SB431542 and galunisertib on R-SMAD2/3, because SB431542 targets both SMAD3 and SMAD2 activation (26), whereas galunisertib targets preferentially SMAD2 (35). As expected, SB431542 completely abrogated both pSMAD3 and pSMAD2 in CF^{hTERT} (#5) upon TGFβ1 stimulation, whereas galunisertib downregulated pSMAD2 to a greater extent than pSMAD3 (**Fig. 4H**). In line with the knockdown experiments, the lower pSMAD3 inhibition elicited by galunisertib compared with SB431542 was associated with a significantly higher expression of fibrosis markers (**Fig. 4I** and **J**). However, it should be borne in mind that additional differences in the spectrum of targets of these two drugs could also contribute to their distinct antifibrotic effects.

To further validate our observations, we knocked down either *SMAD3* or *SMAD2* in immortalized ADC-TAFs and SCC-TAFs, respectively, from randomly selected patients, using both shRNA and siRNA (Supplementary Materials). In agreement with the results in CFs, shSMAD3 in ADC-TAF^{hTERT} (#13) elicited an SCC-like phenotype in terms of TGFβ signaling, for it significantly decreased both *SMAD3*/*SMAD2* mRNA ratio (**Fig. 4K**) and pSMAD3/pSMAD2 ratio (**Fig. 4L**) compared with control shRNA. Likewise, shSMAD3 in ADC-TAF^{hTERT} downregulated their TGFβ1-induced expression of fibrosis markers (**Fig. 4M** and **N**). In contrast, shSMAD2 in SCC-TAF^{hTERT} (#22) had the opposite effects, eliciting an ADC-like phenotype in terms of TGFβ signaling (**Fig. 4O** and **P**) and fibrosis (**Fig. 4Q** and **R**). Similar results were found in ADC-TAFs and SCC-TAFs from other patients (Supplementary Fig. S5A–S5D) as well as using siRNA (Supplementary Fig. S5E–S5H). Altogether, these results confirm that conditions that favor pSMAD3 over pSMAD2 signaling as in ADC-TAFs (therefore eliciting a ratio pSMAD3/pSMAD2 > 1 as in shSMAD2 or galunisertib) elicit larger expression of fibrosis markers in response to TGFβ1 compared with those conditions that impair pSMAD3 as observed in SCC-TAFs (therefore eliciting a ratio pSMAD3/pSMAD2 < 1 as in shSMAD3). In addition, these results provide additional support to the regulation of R-SMAD2/3 activation

Figure 3.

Histotype-specific expression of fibrosis markers. **A,** Representative Western blot of αSMA, P4HA2, and β-actin of TAFs and paired CFs stimulated with 2.5 ng/mL TGFβ1 for 3 days (Western blot from other patients is shown in Supplementary Fig. S3A and S3B). **B** and **C,** Densitometry analysis expressed as fold (TAF/CF) of αSMA/β-actin (**B**) and P4HA2/β-actin (**C**; 6 ADC, 5 SCC; TAFs and CFs). **D** and **E,** Fold *COL1A1* (**D**) and *TGFB1* (**E**) mRNA (TAF/CF) in cells cultured as in **A** (5-6 ADC, 5 SCC; TAFs and CFs). **F,** Bioactivity of the TGFβ1 secreted into the conditioned medium by TAFs (5 ADC, 4 SCC) cultured as in **A** and kept in culture medium without exogenous TGFβ1 for 48 hours. **G** and **H,** Representative histologic images of ADC and SCC patient samples within TMAs from the CIBERES cohort stained for fibrillar collagens by PSR (**G**) and αSMA (**H**). Patients were stratified in three groups: never smokers, ADC-smokers, and SCC-smokers (current and former). **I–L,** Quantification of the percentage of either PSR or αSMA–positive area/10× field for each patient (112 ADC, 96 SCC) from the CIBERES cohort, which is referred to as PSR% (**I**) and αSMA% (**K**) here and thereafter. **J,** PSR% assessed in TMA samples from the CIMA-CUN cohort (77 ADC, 54 SCC). **L,** Scatter plot of PSR% versus αSMA% for each patient of the CIBERES cohort. Solid lines correspond to a linear model estimated with the intercept set at 0. Interaction of the slope with the histotype assessed with the likelihood ratio test. ###, $P < 0.005$. **M–O,** RNA-seq data of *ACTA2* (**M**), *P4HA2* (**N**), and *COL1A1* (**O**) from TCGA samples (101 ADC, 81 SCC). **P,** Representative SHG images of ADC and SCC patients. **Q,** Outcome of the CT-FIRE software applied on the images shown in **P**; labeling each individually detected filament. **R,** Average number of filaments/40 × field in ADC ($n = 8$) and SCC ($n = 7$) patients assessed as in **Q**. A single value was discarded using Grubbs outlier test in **B** and **C** (further details in Supplementary Fig. S3C). *, $P < 0.05$ was determined by comparing ADC- or SCC-smokers with never smokers using Student *t* test (**I–L**) or Wilcoxon rank-sum test (**M–O**). All other statistical analyses as in **Fig. 1**. #, $P < 0.05$.

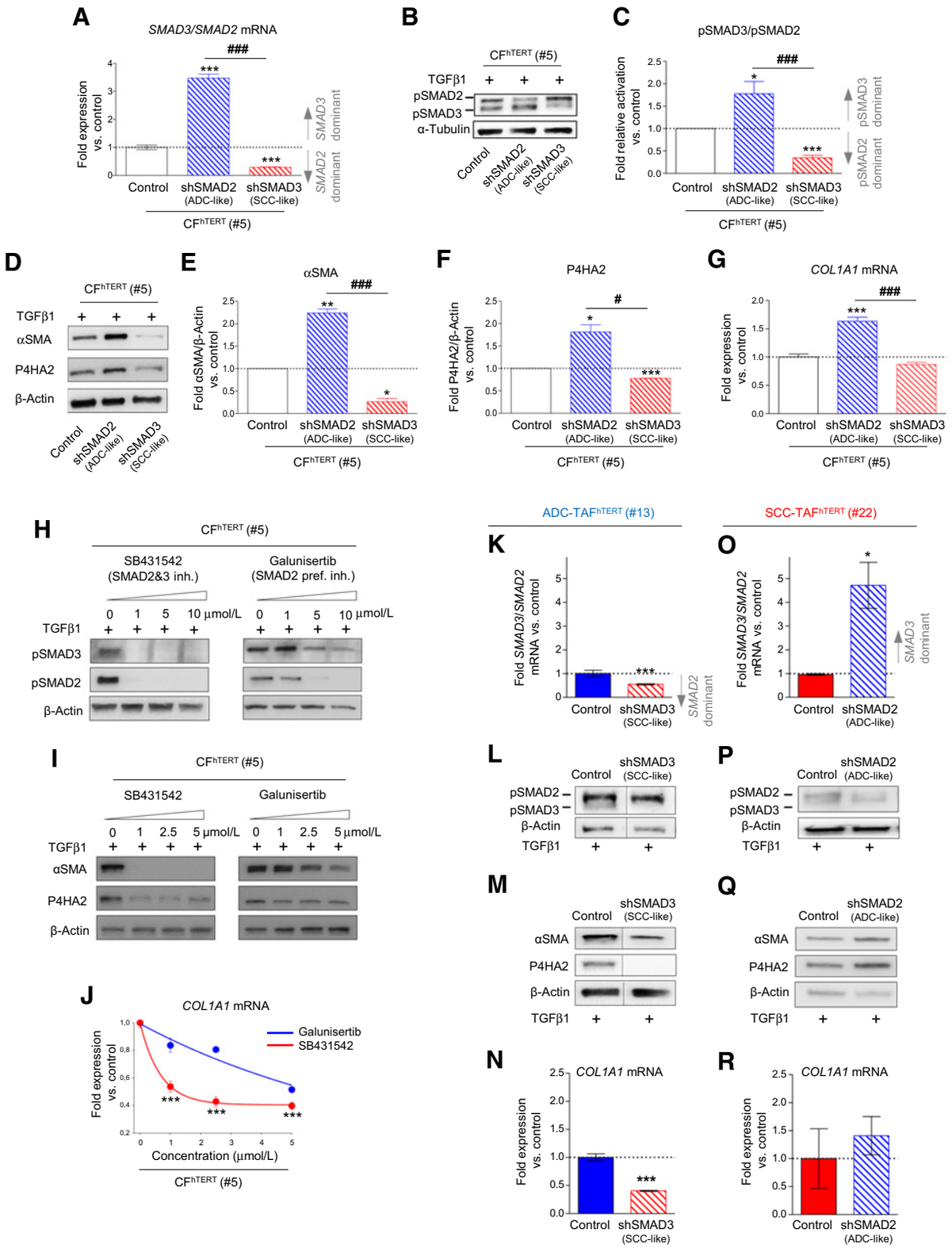

based on a competition/compensation process, because a forced decrease in *SMAD2* mRNA with shSMAD2 was sufficient to increase the pSMAD3/pSMAD2 ratio and the fibrotic phenotype, and vice versa.

Knocking down SMAD3 in ADC-TAFs is sufficient to induce a SCC-like phenotypic switch in terms of their response to the antifibrotic drug nintedanib

Nintedanib is a stromal multikinase inhibitor of VEGFR, PDGFR, and FGFR (36) that has been approved as a second-line treatment for patients with ADC without targetable mutations by the EMA (37), and as a first-line treatment for idiopathic pulmonary fibrosis by the EMA and the FDA (38), based on the LUME-Lung clinical trial (13) and the INPULSIS clinical trial (39), respectively. Owing to our observed low SMAD3 expression and activation selectively in SCC-TAFs, concomitantly with their moderate fibrotic phenotype, we sought to determine whether such low TGFβ/SMAD3 signaling could underlie the poor therapeutic effects of nintedanib observed in SCC-TAFs compared with ADC-TAFs (12). To this aim, we first examined the impact of nintedanib on R-SMAD2/3 and nuclear SMAD4 in CF^{hTERT} (#5 or #37), and found that it markedly inhibited both the activation of R-SMAD2/3 (**Fig. 5A–C**) and the increase in nuclear SMAD4 (**Fig. 5D** and **E**) in response to TGFβ1, yet not as efficiently as SB431542 (**Fig. 1A** and **B**), which specifically targets ALK5 and other type I TGFβ receptors (**Fig. 4H–J**; ref. 26), thereby supporting that ALK5 may be an off-target of nintedanib (40). To check this possibility, we performed a time-course analysis of phospho-ALK5 (pALK5) and pSMAD3 in CF^{hTERT} (#5) in response to TGFβ1 with or without nintedanib (**Fig. 5F**). As expected, the peak in pALK5 induced by TGFβ1 occurred before that of pSMAD3; moreover, nintedanib downregulated pALK5 but not total ALK5, supporting that ALK5 is an unintended target of this drug.

Next, we examined the responses to nintedanib in immortalized ADC-TAFs from two randomly selected patients (#12 and #13) after knocking down *SMAD3* by shRNA, which elicited a significant decrease in *SMAD3*/*SMAD2* mRNA ratio (**Fig. 5G**). Remarkably, knocking down SMAD3 in ADC-TAF^{hTERT} (#12) was sufficient to elicit a smaller nintedanib reduction in the expression of an extended panel of fibrosis markers (i.e., *COL1A1* mRNA, *COL3A1* mRNA, αSMA, and TGFβ1 activity; **Fig. 5H–L**) in response to TGFβ1 compared with control shRNA, which closely resembled the significantly smaller inhibitory effects of nintedanib on SCC-TAFs compared with ADC-TAFs (**Fig. 5H–L**). Likewise, the lack of differential nintedanib reduction of the expression of P4HA2 between control shRNA and shSMAD3 in ADC-TAF^{hTERT} (#12) mimicked the lack of distinct responses between ADC-TAFs and SCC-TAFs (**Fig. 5K**). Consistently, knocking down *SMAD3* in ADC-TAFs (#12) impaired the growth inhibition of the EGFR wild-type ADC cancer cell line H1437 elicited by the CM of TGFβ1-activated fibroblasts in the presence of nintedanib compared with control ADC-TAFs (**Fig. 5M** and **N**), similarly to the lower growth reduction elicited by the CM of nintedanib-treated SCC-TAFs compared with ADC-TAFs (**Fig. 5N**). Comparable results were obtained in ADC-TAF^{hTERT} (#13) using different plasmids (Supplementary Fig. S6A and S6B). Collectively, these results reveal that knocking down *SMAD3* in ADC-TAFs is sufficient to render a SCC-like phenotype in terms of both the antifibrotic and antigrowth responses to nintedanib *in vitro*.

Knocking down SMAD3 in CFs coinjected with ADC cancer cells is sufficient to abrogate the antitumor response to nintedanib *in vivo*

To validate the prominent role of SMAD3 in modulating the therapeutic responses of ADC-TAFs to nintedanib *in vivo*, we coinjected subcutaneously H1437 cells with either control shRNA or shSMAD3 CF^{hTERT} (#5) into NOD/SCID mice. CF^{hTERT} were preactivated before coinjection with TGFβ1 to mimic the profibrotic phenotype of TAFs found in patients (**Fig. 6A**; ref. 14), and were used instead of ADC-TAF^{hTERT} owing to technical difficulties in expanding these cells up to the large numbers required for *in vivo* experiments. Two weeks postinjection, tumor-bearing mice (size $\geq$ 50 mm^3) were treated with nintedanib or PBS during 2 weeks. In agreement with our *in vitro* data, nintedanib elicited significant antitumor growth effects (**Fig. 6B**) and delayed tumor engraftment (**Fig. 6C**) in H1437 cancer cells coinjected with control, but not shSMAD3 fibroblasts. Moreover, nintedanib reduced both the expression of fibrillar collagens and the percentage of proliferating ($Ki\text{-}67^+$) cancer cells to a much greater extent in tumor-bearing control compared with shSMAD3 fibroblasts (**Fig. 6D–F**). These results reveal that knocking down SMAD3 in fibroblasts is sufficient to scale down tumor growth and fibrosis as well as to impair the antitumor growth and antifibrotic effects of nintedanib in primary tumor xenografts, thereby mimicking the negative therapeutic responses reported in patients with SCC (13).

Discussion

We recently reported the seemingly paradoxical observation that NSCLC is highly fibrotic, even though the profibrotic transcription factor *SMAD3* is epigenetically downregulated through promoter hypermethylation in TAFs compared with paired CFs derived from patients with both ADC and SCC (11). Here we shed light on this apparent paradox by reporting for the first time that tumor fibrosis is actually higher in ADC than SCC, and by providing novel insights on

Figure 4.

Modulation of TGFβ1-induced fibrosis upon the loss of function of pSMAD3 or pSMAD2. Experiments were conducted using hTERT immortalized CFs or TAFs (Supplementary Fig. S7A–S7D), which did not compromise their TGFβ1 responses (Supplementary Fig. S7E–S7I). **A,** Fold *SMAD3*/*SMAD2* mRNA ratio of shSMAD2 and shSMAD3 fibroblasts with respect to control shRNA fibroblasts maintained in culture medium supplemented with 10% FBS. **B,** Representative Western blot of pSMAD2, pSMAD3, and α-tubulin of control, shSMAD2, and shSMAD3 fibroblasts stimulated with 2.5 ng/mL TGFβ1 for 60 minutes. **C,** Densitometry analysis expressed as fold of pSMAD3/pSMAD2 from fibroblasts cultured as in **B**. **D,** Representative Western blot of αSMA, P4HA2, and β-actin of control, shSMAD2, and shSMAD3 fibroblasts stimulated with 2.5 ng/mL TGFβ1 for 3 days. **E** and **F,** Densitometry Western blot analysis expressed as fold of αSMA/β-actin (**E**) and P4HA2/β-actin (**F**) of fibroblasts cultured as in **D**. **G,** Fold *COL1A1* mRNA of fibroblasts stimulated with 2.5 ng/mL TGFβ1 for 2 days. **H,** Representative Western blot for pSMAD2, pSMAD3, and β-actin of control fibroblasts cultured as in **B** in the presence of SB431542 or galunisertib. **I,** Representative Western blot for αSMA, P4HA2, and β-actin of control fibroblasts cultured as in **D** and treated with SB431542 or galunisertib. **J,** Fold *COL1A1* mRNA of control fibroblasts cultured as in **I**. **K–R,** effect of either shSMAD3 on ADC-TAFs or shSMAD2 on SCC-TAFs in terms of the *SMAD3*/*SMAD2* mRNA ratio (**K** and **O**), activation of R-SMAD2/3 (**L** and **P**), and the expression of fibrosis markers (**M–R**). TAFs were cultured as in **B** and **D** to assess R-SMAD2/3 and fibrosis markers, respectively. Similar results were obtained in TAFs from other patients and with siRNA (Supplementary Fig. S5 and Supplementary Materials). #, $P < 0.05$; ###, $P < 0.005$ comparing shSMAD2 and shSMAD3 models; *, $P < 0.05$; **, $P < 0.01$; ***, $P < 0.005$ comparing either shSMAD2 or shSMAD3 with control shRNA (**A**, **C**, **E–G**, **K–L**, and **Q–R**) or SB431542 with galunisertib (**N**); mean values correspond to $n \geq 2$ experiments.

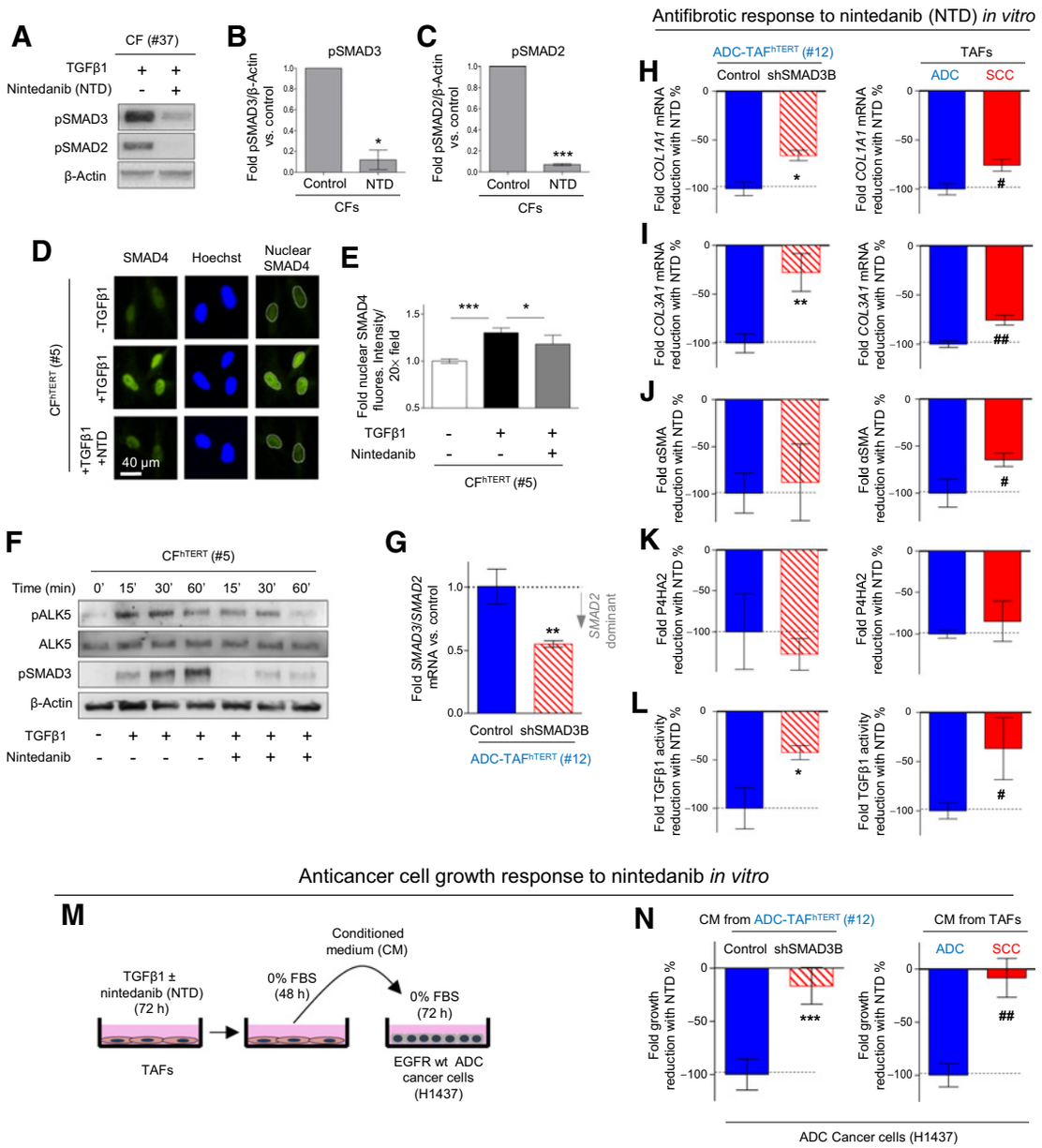

Figure 5.

Role of SMAD3 in the antifibrotic and anticancer effects of nintedanib in TAFs *in vitro*. **A,** Representative Western blot of pSMAD2, pSMAD3, and β-actin of CFs cultured as in **Fig. 4B** with our without 2 μmol/L nintedanib. **B** and **C,** Average densitometry analysis expressed as fold of pSMAD3/β-actin (**B**) and pSMAD2/β-actin (**C**) of CFs (#5 and #37). **D** and **E,** Representative fluorescence images of nuclear SMAD4 of CFs (**D**) cultured as in **A** and corresponding quantification (**E**). **F,** Representative Western blot of the time-course of total and phospho-ALK5, pSMAD3, and β-actin of CFs cultured as in **A** with our without 2 μmol/L nintedanib. **G,** Fold *SMAD3/SMAD2* mRNA ratio of ADC-TAF^{hTERT} transduced with shSMAD3 or control shRNA and maintained as in **Fig. 4A**. **H–L,** Fold relative reduction of a panel of fibrosis markers including *COL1A1* mRNA (**H**), *COL3A1* mRNA (**I**), αSMA/β-actin (**J**), P4HA2/β-actin (**K**), and TGFβ1 activity (**L**) in either control or shSMAD3 ADC-TAF^{hTERT} or TAFs ($n = 5$–6 ADC; $n = 5$–8 SCC) upon stimulation with 2.5 ng/mL TGFβ1 with or without 2 μmol/L nintedanib for 3 days. TGFβ1 activity was assessed as in **Fig. 3F**. For each marker, fold relative reduction was computed as $100(E_{nintedanib} - E)/E$, where $E_{nintedanib}$ and E are the average expression with or without nintedanib, respectively. **M,** Outline of the experimental design used to assess the growth of H1437 cancer cells stimulated with CM from TAFs activated as in (**H–L**) and maintained in serum-free and nintedanib-free fibroblast culture medium for 48 hours. **N,** Fold relative reduction in cell number/10× field of H1437 cells stimulated with CM from either control or shSMAD3 ADC-TAF^{hTERT} (**J**) or TAFs (4 ADC, 4 SCC). Fold relative reduction in cell growth was computed as in **H–L**. The H1437 cell line was chosen to mimic the EGFR wild-type (wt) status of patients with ADC that may be treated with nintedanib in clinical settings. *, $P < 0.05$; ***, $P < 0.005$ comparing either nintedanib treated with untreated fibroblasts or shSMAD3 with control ADC-TAFs. #, $P < 0.05$; ##, $P < 0.01$ comparing ADC-TAFs and SCC-TAFs; mean values correspond to $n = 2$ independent experiments. *, $P < 0.05$; **, $P < 0.01$; ***, $P < 0.005$.

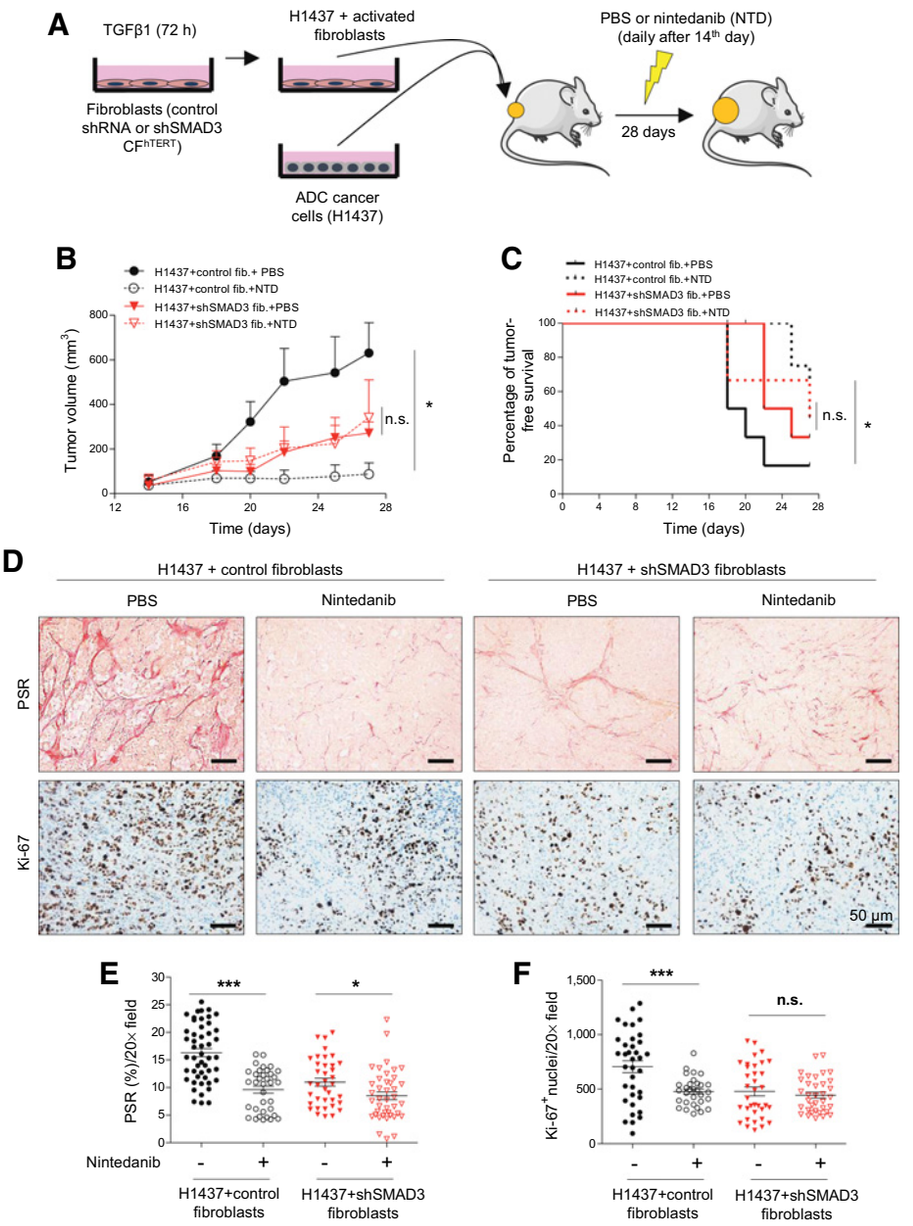

Figure 6.

Regulatory role of SMAD3 in the antifibrotic and anticancer cell growth effects of nintedanib in fibroblasts *in vivo*. **A,** Outline of the experimental design used to assess tumor growth of H1437 cells subcutaneously coinjected with control shRNA or shSMAD3 CF^{hTERT} (#5; 2:1 ratio) into immunodeficient NOD/SCID mice. Fibroblasts were preactivated with 2.5 ng/mL TGFβ1 for 3 days before coinjection. Two weeks postinjection, mice were treated daily with nintedanib or PBS by oral gavage during 2 weeks ($n = 6$ mice per condition). **B,** Average tumor growth for each experimental condition. **C,** Percentage of tumor-free mice (tumors < 200 mm^3). **D,** Representative images of PSR (top) and Ki-67 (bottom) staining at the end of the observation period. **E** and **F,** Quantification of the percentage of the PSR-positive area (**E**) or Ki-67$^+$ nuclei/20× field (**F**) for each image and mice ($n = 12$ images/tumor). Two group comparisons between absence or presence of nintedanib were performed with two-way ANOVA (**B**), log-rank test (**C**), or Student *t* test (**E** and **F**). *, $P < 0.05$; ***, $P < 0.005$; n.s. nonsignificant.

key underlying mechanisms. Specifically, unlike ADC-TAFs, the *SMAD3* promoter in SCC-TAFs was strongly hypermethylated with respect to paired CFs, which was consistently associated with a much lower *SMAD3* expression and activation in response to TGFβ1 that was compensated by an enhanced SMAD2 activation. Conversely, a global demethylating agent was sufficient to rescue the *SMAD3* mRNA expression and protein activation in SCC-TAFs but not in paired CFs, thereby supporting that DNA hypermethylation is a major driving process of the *SMAD3* transcriptional repression in SCC-TAFs. Of note, the low *SMAD3* mRNA expression of SCC-TAFs elicited a response to TGFβ1 dominated by SMAD2 rather than SMAD3, and yielded a significantly lower expression of fibrosis markers compared with ADC-TAFs *in vitro* that was confirmed in three patient cohorts. Conversely, knocking down *SMAD2* in SCC-TAFs rescued both TGFβ1/SMAD3 activation and the expression of fibrosis markers. In line with our findings, although it remains technically challenging to validate in patient samples our *in vitro* observation of a larger ratio of SMAD3/SMAD2 expression and phosphorylation in ADC-TAFs than in SCC-TAFs, previous IHC analyses reported lower stromal staining of total SMAD3 in SCC compared with ADC (31), and an opposite histologic pattern of pSMAD2 (41).

We also report the novel observation that ADC-TAFs were hyperresponsive to TGFβ1 in terms of overexpressing a panel of fibrosis markers compared with both patient-matched CFs and SCC-TAFs. The hypertrophic phenotype of ADC-TAFs was associated with a moderate hypermethylation of the *SMAD3* promoter, with both a *SMAD3* mRNA and a pSMAD3/pSMAD2 ratio above basal values, and with a larger activity of endogenous TGFβ1, which elicited a

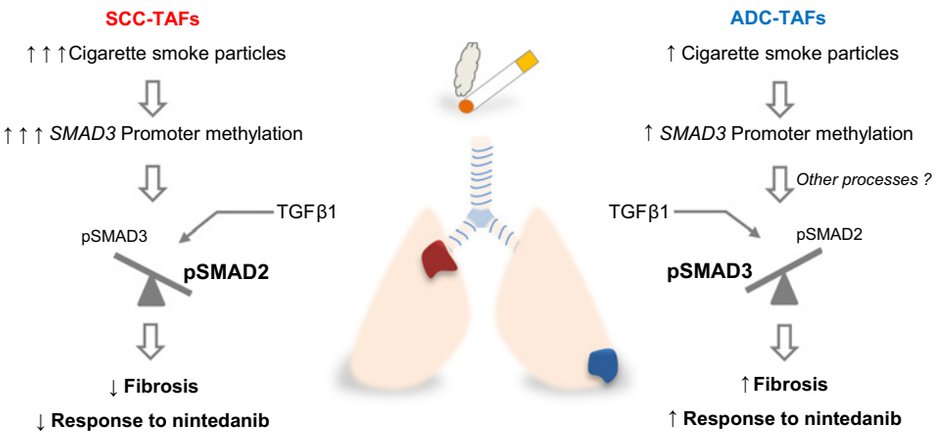

Figure 7.
Emerging model supporting a link between smoking, the anatomic location of ADC and SCC, and the differential *SMAD3* promoter methylation, SMAD3/SMAD2 balance, fibrosis, and response to the antifibrotic drug nintedanib in ADC-TAFs and SCC-TAFs.

response to TGFβ1 that was dominated by SMAD3 over SMAD2. Consistently, knocking down *SMAD3* abrogated the hypertrophic phenotype of ADC-TAFs. The underlying mechanisms of such hypertrophic phenotype remain an open question. However, our observed larger autoinduction of TGFβ1 selectively in ADC-TAFs in response to exogenous TGFβ1 provides a straightforward process to amplify profibrotic TGFβ responses. Nonetheless, all these observations are consistent with the acknowledged prominent profibrotic role of SMAD3 elicited by TGFβ1. Moreover, they are in agreement with the stronger association between glucose uptake and the fibrotic stroma that has been reported in ADC compared with SCC (42), which could account for the metabolic demands required for the increased collagen deposition that we observed in ADC.

The selective hyperactivation of pSMAD2 in SCC-TAFs in response to TGFβ1 was not anticipated, for their *SMAD2* mRNA levels were comparable with paired CFs and ADC-TAFs. In line with this observation, knocking down SMAD3 in TAFs and CFs elicited a larger SMAD2 activation concurrently with a downregulation of the expression of fibrosis markers, whereas knocking down SMAD2 elicited opposite effects. In agreement with our findings, knocking out SMAD2 in mouse embryonic fibroblasts enhanced the expression of common SMAD3-regulated profibrotic genes, the nuclear translocation of pSMAD3, and the binding of SMAD3 to the *COL1A2* promoter in response to TGFβ1. In contrast, knocking out SMAD3 attenuated all these effects (28, 43). Because the activation of both SMAD3 and SMAD2 requires phosphorylation by ALK5 and subsequent binding to SMAD4 (25, 28, 29), the latter observations and ours support that the activations of SMAD2 and SMAD3 in response to TGFβ1 are not independent but rather they are coregulated by their mutual competition for interacting with common factors like ALK5 and SMAD4.

Defining the causes underlying the larger *SMAD3* promoter hypermethylation in SCC-TAFs compared with ADC-TAFs remains to be fully elucidated. Yet, our results and other lines of evidence support that smoking and the frequent anatomic location of SCC in the proximal airways (44) may play a major role. Thus, smoking is more strongly associated with SCC than ADC (3, 44), and the highest deposition of cigarette smoke particles has been documented in the proximal airways where SCC tumors are commonly found, whereas the same tobacco consumption elicits the deposition of fewer and smaller cigarette smoke particles in distal pulmonary sites where ADC tumors are frequently located (3, 32). Moreover, we showed that long-term exposure to CSC alone can increase the promoter methylation of *SMAD3* but not *SMAD2* in pulmonary fibroblasts, which is remarkable because smoking is known to induce global hypomethylation (45). Likewise, others have reported that total tumor *SMAD3* mRNA was lower in smokers compared with never-smokers in patients with NSCLC (31). In addition, we reported a lower collagen deposition in SCC-smokers compared with both ADC-smokers and never smokers in two independent patient cohorts. All these observations support an emerging model (**Fig. 7**) that considers an increased exposure to cigarette smoke particles in SCC-TAFs compared with ADC-TAFs (due to their anatomic location, increased tobacco consumption, or both), which favors pSMAD2 over pSMAD3 through increased *SMAD3* epigenetic repression, owing to a compensation process based on their competition for common cofactors. In turn, the low pSMAD3/pSMAD2 ratio of SCC-TAFs impairs tumor fibrosis and their response to the antifibrotic drug nintedanib. This model provides also a rationale for the puzzling epidemiologic observation that smoking is associated with lower risk of radiotherapy-induced pneumonitis/fibrosis in NSCLC, whereas tumors located in the lower lobes have a higher risk (46). However, we cannot rule out that biological effects other than smoking and anatomic location may contribute also to the distinct fibrotic phenotypes of SCC-TAFs and ADC-TAFs, including potential distinct cell lineages, intrinsic regional features, or even the epigenetic reprogramming of TAFs through their crosstalk with cancer cells (11, 47, 48).

Finally, it is worth noting that our findings may have far reaching translational implications beyond the identification of the low SMAD3 activation of SCC-TAFs as a potential key process underlying the poor sensitivity to nintedanib reported in patients with SCC in the LUME-1 trial (13). First, the larger tumor fibrosis of ADC compared with SCC strongly suggests that ADC tumors could be more responsive to antifibrotic therapies, in agreement with the stronger *in vitro* therapeutic responses to nintedanib of ADC-TAFs compared with SCC-TAFs reported here and elsewhere (12). Second, our results support that nintedanib (and possibly other antifibrotic drugs) may be particularly useful in overcoming the unwanted radiotherapy-induced fibrosis in ADC, which is a major resistance mechanism (15) that has been linked with increased levels of circulating TGFβ (49).

In summary, our work reveals that the phenotypic heterogeneity of TAFs in NSCLC (48) strongly depends on their histologic subtype in terms of TGFβ1/SMAD3 signaling, fibrosis regulation and response to nintedanib, and it is intimately associated with a marked epigenetic repression of *SMAD3* that favors pSMAD2 over pSMAD3 selectively in SCC-TAFs. The latter process emerges as a critical mechanism for the limited tumor fibrosis and negative response to the antifibrotic drug nintedanib in SCC compared with ADC.

Disclosure of Potential Conflicts of Interest

R. Ikemori reports receiving a commercial research grant from Boehringer Ingelheim. L. Soucek is a CEO at Peptomyc SL. F. Hilberg is a senior scientific expert at Boehringer Ingelheim RCV. N. Reguart reports receiving a commercial research grant from Pfizer and Novartis, has received speakers bureau honoraria from Pfizer, Roche, MSD, Boehringer, Bristol-Myers Squibb, AstraZeneca, and is a consultant/advisory board member for Pfizer, MSD, Boehringer, and AstraZeneca. J. Alcaraz reports receiving a commercial research grant from Boehringer-Ingelheim. No potential conflicts of interest were disclosed by the other authors.

Authors' Contributions

Conception and design: R. Ikemori, F. Hilberg, N. Reguart, J. Alcaraz
Development of methodology: R. Ikemori, M. Gabasa, P. Duch, P. Bragado, A. Marín, G. Fuster, S. Gea-Sorli, T. Jauset, L. Soucek, M. Esteller, J. Alcaraz
Acquisition of data (provided animals, acquired and managed patients, provided facilities, etc.): R. Ikemori, M. Gabasa, P. Duch, A. Marín, S. Morán, L.M. Montuenga, M. Esteller, E. Monsó, V.I. Peinado, C. Fillat, N. Reguart, J. Alcaraz
Analysis and interpretation of data (e.g., statistical analysis, biostatistics, computational analysis): R. Ikemori, M. Gabasa, P. Duch, M. Vizoso, M. Arshakyan, I.-C. Luis, A. Marín, M. Castro, M. Esteller, P. Gascon, J. Alcaraz
Writing, review, and/or revision of the manuscript: R. Ikemori, P. Duch, M. Vizoso, P. Bragado, A. Marín, G. Fuster, L. Soucek, L.M. Montuenga, E. Monsó, M. Esteller, P. Gascon, C. Fillat, F. Hilberg, N. Reguart, J. Alcaraz
Administrative, technical, or material support (i.e., reporting or organizing data, constructing databases): R. Ikemori, L.M. Montuenga, M. Esteller, J. Alcaraz
Study supervision: R. Ikemori, V.I. Peinado, J. Alcaraz
Other (manuscript review): M. Gabasa

Acknowledgments

We thank Maria Calvo, Lara Sedó, Josep Marimón (CCiTUB), Raquel Bermudo (IDIBAPS), Kyla Driscoll (Eli Lilly), Núria de-la-Iglesia, Leire Pedrosa, Iñaki Martín-Subero (IDIBAPS), Meritxell Mollà, David Sánchez, Cristina Teixidó, Daniel Martínez, Josep Ramírez (Hospital Clínic), Alexandre Calon (IMIM), Elena Sancho (IRB), Carolina Francelin (University of Alabama, Birmingham, AL), Natalia Díaz, Alejandro Llorente, Isabel Fabregat, Josep Lluis Carrasco, Daniel Navajas and Ramon Farré (UB), and Cooperative Lung Cancer Group CIBERES-CIBERONC-SEPAR-Biobanco (Supplementary Materials) for technical support and discussions. This work was supported by grants from the Ministerio de Economía y Competitividad (MINECO/FEDER, UE; PI13/02368 and SAF2016-79527-R to J. Alcaraz; BIO2014-57716-C2-2-R and BIO2017-89754-C2-2R to C. Fillat; CB16/12/00312 to M. Esteller; FIS PI15/00167 to E. Monsó; FIS PI16/01821 to L.M. Montuenga), Fundació Privada Cellex (to J. Alcaraz), Generalitat de Catalunya (AGAUR SGR 661 and CERCA Programme to J. Alcaraz; SGR 716 to E. Monsó), Asociación Española Contra el Cáncer (B16-917 to J. Alcaraz; GCB14-2170 to L.M. Montuenga), SEPAR (437 to N. Reguart; PII Oncología Torácica to E. Monsó), and fellowships from Ciência sem Fronteiras (232704/2014-7 to R. Ikemori) and UB/APIF (to P. Duch).

The costs of publication of this article were defrayed in part by the payment of page charges. This article must therefore be hereby marked *advertisement* in accordance with 18 U.S.C. Section 1734 solely to indicate this fact.

Received February 22, 2019; revised September 13, 2019; accepted October 29, 2019; published first November 6, 2019.

References

1. Siegel RL, Miller KD, Jemal A. Cancer statistics, 2018. CA Cancer J Clin 2018;68:7–30.
2. Torre LA, Bray F, Siegel RL, Ferlay J, Lortet-Tieulent J, Jemal A. Global cancer statistics, 2012. CA Cancer J Clin 2015;65:87–108.
3. Chen Z, Fillmore CM, Hammerman PS, Kim CF, Wong K-K. Non-small-cell lung cancers: a heterogeneous set of diseases. Nat Rev Cancer 2014;14:535–46.
4. Ohlund D, Elyada E, Tuveson D. Fibroblast heterogeneity in the cancer wound. J Exp Med 2014;211:1503–23.
5. Navab R, Strumpf D, Bandarchi B, Zhu CQ, Pintilie M, Ramnarine VR, et al. Prognostic gene-expression signature of carcinoma-associated fibroblasts in non-small cell lung cancer. Proc Natl Acad Sci U S A 2011;108:7160–65.
6. Soltermann A, Tischler V, Arbogast S, Braun J, Probst-Hensch N, Weder W, et al. Prognostic significance of epithelial-mesenchymal and mesenchymal-epithelial transition protein expression in non-small cell lung cancer. Clin Cancer Res 2008;14:7430–37.
7. Alcaraz J, Carrasco JL, Millares L, Luis I-C, Fernández-Porras FJ, Martínez-Romero A, et al. Stromal markers of activated tumor associated fibroblasts predict poor survival and are associated with necrosis in non-small cell lung cancer. Lung Cancer 2019;135:151–60.
8. Scotton CJ, Chambers RC. Molecular targets in pulmonary fibrosis - The myofibroblast in focus. Chest 2007;132:1311–21.
9. Sterlacci W, Wolf D, Savic S, Hilbe W, Schmid T, Jamnig H, et al. High transforming growth factor beta expression represents an important prognostic parameter for surgically resected non-small cell lung cancer. Hum Pathol 2012;43:339–49.
10. Bonniaud P, Kolb M, Galt T, Robertson J, Robbins C, Stampfli M, et al. Smad3 null mice develop airspace enlargement and are resistant to TGF-beta-mediated pulmonary fibrosis. J Immunol 2004;173:2099–108.
11. Vizoso M, Puig M, Carmona FJ, Maqueda M, Velásquez A, Gómez A, et al. Aberrant DNA methylation in non small cell lung cancer associated fibroblasts. Carcinogenesis 2015;36:1453–63.
12. Gabasa M, Ikemori R, Hilberg F, Reguart N, Alcaraz J. Nintedanib selectively inhibits the activation and tumor-promoting effects of fibroblasts from lung adenocarcinoma patients. Br J Cancer 2017;117:1128–38.
13. Reck M, Kaiser R, Mellemgaard A, Douillard J-Y, Orlov S, Krzakowski M, et al. Docetaxel plus nintedanib versus docetaxel plus placebo in patients with previously treated non-small-cell lung cancer (LUME-Lung 1): a phase 3, double-blind, randomised controlled trial. Lancet Oncol 2014;15:143–55.
14. Puig M, Lugo R, Gabasa M, Gimenez A, Velasquez A, Galgoczy R, et al. Matrix Stiffening and beta(1) integrin drive subtype-specific fibroblast accumulation in lung cancer. Mol Cancer Res 2015;13:161–73.
15. Barker HE, Paget JTE, Khan AA, Harrington KJ. The tumour microenvironment after radiotherapy: mechanisms of resistance and recurrence. Nat Rev Cancer 2015;15:409–25.
16. Abramoff MD, Magelhaes PJ, Ram SJ. Image processing with ImageJ. Biophotonics Int 2004;11:42.
17. Drifka CR, Tod J, Loeffler AG, Liu Y, Thomas GJ, Eliceiri KW, et al. Periductal stromal collagen topology of pancreatic ductal adenocarcinoma differs from that of normal and chronic pancreatitis. Mod Pathol 2015;28:1470–80.
18. Bredfeldt JS, Liu Y, Pehlke CA, Conklin MW, Szulczewski JM, Inman DR, et al. Computational segmentation of collagen fibers from second-harmonic generation images of breast cancer. J Biomed Opt 2014;19:16007.
19. Tura-Ceide O, Lobo B, Paul T, Puig-Pey R, Coll-Bonfill N, Garcia-Lucio J, et al. Cigarette smoke challenges bone marrow mesenchymal stem cell capacities in guinea pig. Respir Res 2017;18:50.
20. Piek E, Westermark U, Kastemar M, Heldin CH, van Zoelen EJ, Nister M, et al. Expression of transforming-growth-factor (TGF)-beta receptors and Smad proteins in glioblastoma cell lines with distinct responses to TGF-beta1. Int J Cancer 1999;80:756–63.
21. Livak KJ, Schmittgen TD. Analysis of relative gene expression data using real-time quantitative PCR and the 2(-Delta Delta C(T)) Method. Methods 2001;25:402–8.
22. Gabasa M, Duch P, Jorba I, Gimenez A, Lugo R, Pavelescu I, et al. Epithelial contribution to the profibrotic stiff microenvironment and myofibroblast population in lung fibrosis. Mol Biol Cell 2017;28:3741–55.
23. Lugo R, Gabasa M, Andriani F, Puig F, Facchinetti F, Ramírez J, et al. Heterotypic paracrine signaling drives fibroblast senescence and tumor progression of large cell carcinoma of the lung. Oncotarget 2016;7:82324–37.
24. Derynck R, Zhang YE. Smad-dependent and Smad-independent pathways in TGF-beta family signalling. Nature 2003;425:577–84.
25. Bierie B, Moses HL. TGF beta: the molecular Jekyll and Hyde of cancer. Nat Rev Cancer 2006;6:506–20.
26. Inman GJ, Nicolas FJ, Callahan JF, Harling JD, Gaster LM, Reith AD, et al. SB-431542 is a potent and specific inhibitor of transforming growth factor-beta superfamily type I activin receptor-like kinase (ALK) receptors ALK4, ALK5, and ALK7. Mol Pharmacol 2002;62:65–74.

27. Koslowski R, Seidel D, Kuhlisch E, Knoch KP. Evidence for the involvement of TGF-beta and PDGF in the regulation of prolyl 4-hydroxylase and lysyloxidase in cultured rat lung fibroblasts. Exp Toxicol Pathol 2003;55: 257–64.
28. Meng XM, Huang XR, Chung ACK, Qin W, Shao X, Igarashi P, et al. Smad2 protects against TGF-beta/Smad3-mediated renal fibrosis. J Am Soc Nephrol 2010;21:1477–87.
29. Yu J, Zhang L, Chen AL, Xiang GX, Wang YH, Wu JP, et al. Identification of the gene transcription and apoptosis mediated by TGF-beta-Smad2/3-Smad4 signaling. J Cell Physiol 2008;215:422–33.
30. Mann J, Oakley F, Akiboye F, Elsharkawy A, Thorne AW, Mann DA. Regulation of myofibroblast transdifferentiation by DNA methylation and MeCP2: implications for wound healing and fibrogenesis. Cell Death Different 2007;14:275–85.
31. Samanta D, Gonzalez AL, Nagathihalli N, Ye F, Carbone DP, Datta PK. Smoking attenuates transforming growth factor-beta-mediated tumor suppression function through downregulation of smad3 in lung cancer. Cancer Prev Res 2012;5: 453–63.
32. Robinson RJ, Yu CP. Deposition of cigarette smoke particles in the human respiratory tract. Aerosol Sci Technol 2001;34:202–15.
33. Zhang W, Ou J, Inagaki Y, Greenwel P, Ramirez F. Synergistic cooperation between Sp1 and Smad3/Smad4 mediates transforming growth factor beta1 stimulation of alpha 2(I)-collagen (COL1A2) transcription. J Biol Chem 2000; 275:39237–45.
34. Piek E, Ju WJ, Heyer J, Escalante-Alcalde D, Stewart CL, Weinstein M, et al. Functional characterization of transforming growth factor beta signaling in Smad2- and Smad3-deficient fibroblasts. J Biol Chem 2001; 276:19945–53.
35. Herbertz S, Sawyer JS, Stauber AJ, Gueorguieva I, Driscoll KE, Estrem ST, et al. Clinical development of galunisertib (LY2157299 monohydrate), a small molecule inhibitor of transforming growth factor-beta signaling pathway. Drug Des Devel Ther 2015;9:4479–99.
36. Hilberg F, Roth GJ, Krssak M, Kautschitsch S, Sommergruber W, Tontsch-Grunt U, et al. BIBF 1120: Triple angiokinase inhibitor with sustained receptor blockade and good antitumor efficacy. Cancer Res 2008;68:4774–82.
37. Bronte G, Passiglia F, Galvano A, Barraco N, Listi A, Castiglia M, et al. Nintedanib in NSCLC: evidence to date and place in therapy. Ther Adv Med Oncol 2016;8:188–97.
38. Wollin L, Wex E, Pautsch A, Schnapp G, Hostettler KE, Stowasser S, et al. Mode of action of nintedanib in the treatment of idiopathic pulmonary fibrosis. Eur Respirat J 2015;45:1434–45.
39. Richeldi L, Costabel U, Selman M, Kim DS, Hansell DM, Nicholson AG, et al. Efficacy of a tyrosine kinase inhibitor in idiopathic pulmonary fibrosis. N Engl J Med 2014;365:1079–87.
40. Rangarajan S, Kurundkar A, Kurundkar D, Bernard K, Sanders YY, Ding Q, et al. Novel mechanisms for the antifibrotic action of nintedanib. Am J Respir Cell Mol Biol 2016;54:51–9.
41. Chen YB, Xing PF, Chen YY, Zou L, Zhang YS, Li F, et al. High p-Smad2 expression in stromal fibroblasts predicts poor survival in patients with clinical stage I to IIIA non-small cell lung cancer. World J Surg Oncol 2014;12:328.
42. Zhang W, Bouchard G, Yu A, Shafiq M, Jamali M, Shrager JB, et al. GFPT2-expressing cancer-associated fibroblasts mediate metabolic reprogramming in human lung adenocarcinoma. Cancer Res 2018;78:3445–57.
43. Zhang L, Liu CW, Meng XM, Huang C, Xu FY, Li J. Smad2 protects against TGF-beta 1/Smad3-mediated collagen synthesis in human hepatic stellate cells during hepatic fibrosis. Mol Cell Biochem 2015;400:17–28.
44. Khuder SA. Effect of cigarette smoking on major histological types of lung cancer: a meta-analysis. Lung Cancer 2001;31:139–48.
45. Smith IM, Mydlarz WK, Mithani SK, Califano JA. DNA global hypomethylation in squamous cell head and neck cancer associated with smoking, alcohol consumption and stage. Int J Cancer 2007;121:1724–8.
46. Kong FM, Wang SL. Nondosimetric risk factors for radiation-induced lung toxicity. Semin Radiat Oncol 2015;25:100–09.
47. Kalluri R. The biology and function of fibroblasts in cancer. Nat Rev Cancer 2016; 16:582–98.
48. Lambrechts D, Wauters E, Boeckx B, Aibar S, Nittner D, Burton O, et al. Phenotype molding of stromal cells in the lung tumor microenvironment. Nat Med 2018;24:1277.
49. Barcellos-hoff MH, Derynck R, Tsang MLS, Weatherbee JA. Transforming growth-factor-beta activation in irradiated marine mammary-gland. J Clin Invest 1994;93:892–99.